Cyclotron Resonance in Uniaxially Stressed Silicon. II. Nature of the Covalent Bond

J. C. HENSEL
Bell Telephone Laboratories, Murray Hill, New Jersey

H. HASEGAWA AND M. NAKAYAMA*
Department of Physics, University of Tokyo, Tokyo, Japan

(Received 8 October 1964)

An energy band of a diamond lattice at $X(\mathbf{k}=(2\pi/a)(1,0,0))$ on the zone boundary is two-fold degenerate because of the presence of glide-reflection symmetries. The degeneracy of the conduction band Δ_1 and $\Delta_{2'}$ at X in silicon was lifted by applying a compressive uniaxial stress along the [011] direction, the effect of which has been observed by measuring a shift of the cyclotron resonance line for the [100] electrons. An expression for the line shift has been obtained in terms of a perturbation series. By evaluating the series using the orthogonal-plane-wave (OPW) results of Kleinman and Phillips, the Δ_1-$\Delta_{2'}$ band mixing ratio $\Xi_{u'}/\Delta E$ is determined to be $\Xi_{u'}/\Delta E=11.4\pm1.1$. This result when combined with OPW estimate for ΔE, the energy separation between Δ_1 and $\Delta_{2'}$ at the conduction band edge, yields the value $\Xi_{u'}\approx5.7$ eV for the deformation potential responsible for the band splitting at X. The lifting of the special degeneracy of the X_1 states is interpreted from the viewpoint of the tetrahedral covalent bond responding to an applied mechanical force. The *sign* of the cyclotron-resonance line shift indicates that two nonbonding orbitals of a valence electron connecting two neighboring Si atoms are hybridized to make the energy of the bonding orbital lower than that of the antibonding orbital when the bond is compressed. Also from the experimental work, the following values of the electron effective masses have been determined: $m_\perp/m=0.1905\pm0.0001$, $m_{\parallel}/m=0.9163\pm0.0004$.

I. INTRODUCTION

IN our previous papers we have presented some theoretical[1] and experimental[2] results of cyclotron resonances on holes in uniaxially stressed silicon crystals. There it has been shown that external uniaxial stresses applied to the crystals bring to light important new features in the microwave resonance spectrum. The present paper is a continuation of the above studies. Here we investigate, both theoretically and experimentally, effects of external stresses on cyclotron resonance *electron* lines in silicon.

The conduction band edge in silicon has been known from various types of experiments to be located on the [100] and equivalent axes (denoted by Δ), very close to the Brillouin zone boundary (the X point). The nature of the conduction band edge is regarded in many respects to be simpler than that of the valence band edge at $\mathbf{k}=0$. There exists, however, one special feature of the conduction band edge which is attributable to the difference between the face-centered cubic and the diamond structures. It is well known that the x-ray scattering factor corresponding to the $\langle 200\rangle$ component in a diamond lattice is forbidden, and that this fact is closely related to the "sticking together" of certain energy bands at the X point.[3] In this paper, we discuss the effect of lattice deformation on the conduction bands in Si. Specifically we consider here the removal of the twofold-band degeneracy of the Δ_1 and $\Delta_{2'}$ bands at X by an application of external uniaxial stresses which cause electron effective-mass shifts due to strain mixing of the electronic wave functions. The resulting effective-mass shifts are detected by cyclotron resonance. A change of optical spectra under strain, perhaps the most direct experimental verification of the effect, has been sought with unsuccessful results.[4] An important advantage of the present method is that by observing cyclotron resonance lines one is able to see the behavior of electrons in each "valley" of the conduction band independently. This enables one to verify the effect by measuring the line shift for a valley chosen at one's option under suitable geometries of stress and magnetic field.

The effect of lifting the band degeneracy has previously been evidenced in the spin-resonance experiments[5] on donors under the [111] stress and also in the theoretical[6,7] and experimental[5] investigations of spin-lattice relaxation mechanisms which were not fully understood in the earlier studies.[8,9] The present work was motivated by these investigations and was undertaken in an attempt to obtain an estimate of the splitting parameter, a new shear deformation potential, $\Xi_{u'}$. The cyclotron resonance technique is perhaps better suited to this problem inasmuch as the response to the applied microwave field is through electric dipoles in which electron spins and spin-orbit interactions are not primarily involved. This fact simplifies theoretical calculations and permits a more direct and accurate

* Present address: College of General Education, University of Tokyo, Meguro-ku, Tokyo, Japan.

[1] H. Hasegawa, Phys. Rev. **129**, 1029 (1963).

[2] J. C. Hensel and G. Feher, Phys. Rev. **129**, 1041 (1963), hereafter referred to as (H-F).

[3] This question was first investigated by F. Hund and B. Mrowka, Ber. Verhandl. Sächs. Akad. Wiss. Leipzig Math.-Phys. Kl. **87**, 185 (1935). See also F. Hund, Z. Physik **99**, 119 (1936).

[4] H. R. Philipp, W. C. Dash, and H. Ehrenreich, Phys. Rev. **127**, 762 (1962) and U. Gerhardt, Phys. Letters **9**, 117 (1964).

[5] D. K. Wilson and G. Feher, Phys. Rev. **124**, 1068 (1961).

[6] L. M. Roth, *Proceedings of the International Conference on Semiconductor Physics, Prague, 1960* (Czechoslovak Academy of Sciences, Prague, 1961), p. 592.

[7] L. Liu, Phys. Rev. **126**, 1317 (1962).

[8] H. Hasegawa, Phys. Rev. **118**, 1523 (1960).

[9] L. M. Roth, Phys. Rev. **118**, 1534 (1960).

analysis of the experimental results than would be possible for the spin-resonance results.

Our theoretical process to deduce $\Xi_{u'}$ from the present experiments is the following: We first make a group-theoretical analysis of symmetry relevant to the X point of the diamond structure, which gives us a way of characterizing the sign of $\Xi_{u'}$ without recourse to very detailed aspects of energy-band calculations. We next utilize results of the current band theory[10] to evaluate a perturbation series that is involved in a theoretical formula for the observed mass shift. We shall be aided by the well-known Phillips "cancellation"[11] between crystal potential and core-orthogonalization terms that makes a nearly free-electron picture suited particularly for electrons in Si. Thus, from the measured cyclotron-resonance line shifts, a ratio $\Xi_{u'}/\Delta E$ which represents a degree of the strain-induced Δ_1-$\Delta_{2'}$ band mixing has been determined. This is combined with a band-theoretical value for ΔE (the Δ_1-$\Delta_{2'}$ separation at the conduction band edge) to give an estimate of $\Xi_{u'}$ which, in turn, may be compared with the direct calculation of Goroff and Kleinman.[12]

From the sign of $\Xi_{u'}$ determined experimentally, a significant conclusion can be drawn. The conduction-band states, when interpreted in terms of tetrahedral, covalent bonds, split under uniaxial stress into a bonding orbital and an antibonding orbital, each characterized by a definite parity. From the orthogonalized-plane-wave (OPW) theory we identify the *bonding* orbital with the state whose energy is *lowered* by the compressive stress which tends to *reduce* the internuclear distance. The OPW calculations further reveal that for the conduction electron the major contributions to the deformation potentials are kinetic in origin.

II. BAND STRUCTURE NEAR $X_1(k=(2\pi/a)(1,0,0))$

A. Symmetries and Selection Rules

Irreducible representations (IR) of the group $G^{\mathbf{k}}$ of $\mathbf{k}=(2\pi/a)(1,0,0)$, for the diamond structure have been determined by several authors.[13,14] There are four inequivalent IR's denoted by X_1, X_2, X_3, and X_4 each doubly degenerate (without spin) as crystal eigenstates. This degeneracy is characteristic of a diamond-type crystal whose unit cell contains two equivalent atoms. It is possible to lift this degeneracy by subjecting the crystal to a large, external uniaxial stress along appropriate crystallographic directions. The conduction band edge in silicon is known to be close to one of the representations X_1. Therefore, the effect of lifting the degeneracy at this point may be observable in a shift of cyclotron-resonance electron line with stresses. We examine this possibility by selecting necessary matrix elements.

Let us define a unit cell in the usual way by introducing three vectors;

$$\mathbf{t}_1=\left(\frac{a}{2},\frac{a}{2},0\right),\quad \mathbf{t}_2=\left(0,\frac{a}{2},\frac{a}{2}\right),\quad \mathbf{t}_3=\left(\frac{a}{2},0,\frac{a}{2}\right),$$

where a is the lattice constant, and assume one of the two equivalent atoms to be located at the origin. The position of the other atom is then $\tau=(a/4, a/4, a/4)$. Because of this structure the symmetry operations pertinent to the point $(2\pi/a)(1,0,0)$ contain the inversion followed by a nonprimitive translation τ, which is denoted by $\{I|\tau\}$. This operation must multiply each of the eight point-symmetry operations which makes the $\mathbf{k}$ vector invariant, viz., the point group D_{2d}, to obtain an extended group whose IR's yield all the X_j's. The process is not simply a direct product, because the τ vector is nonprimitive and the $\mathbf{k}$ vector is located at a zone boundary. For every point operation $\{\beta|0\}$ of D_{2d} the operation $\{I|\tau\}$ satisfies the following[14]:

$$\begin{aligned}\{I|\tau\}\{\beta|0\}&=\{\beta I|\tau\}\\ \{\beta|0\}\{I|\tau\}&=\{\beta I|\beta\tau\}\\ &=\{\beta I|\tau\}\{E|\beta^{-1}\tau-\tau\}.\end{aligned}\tag{1}$$

In the last equality $\{E|\beta^{-1}\tau-\tau\}$ is a primitive translation which can be represented by a single phase factor

$$\exp(i\mathbf{k}\cdot(\beta^{-1}\tau-\tau))=\pm 1 \quad \text{for} \quad \mathbf{k}=(2\pi/a)(1,0,0),\tag{2}$$

where $+$ and $-$ signs correspond, respectively, to whether

$$\beta\mathbf{k}=\mathbf{k}=(2\pi/a)(1,0,0),\tag{3}$$

or

$$\beta\mathbf{k}=\mathbf{k}+\mathbf{K}=(2\pi/a)(-1,0,0).\tag{3'}$$

The former relation (3) is satisfied by the four point operations of D_{2d} i.e., by E, C_{2x}, σ_{dyz}, and $\sigma_{d\bar{y}z}$, while the latter relation (3') by the other four i.e., by C_{2y}, C_{2z}, S_{4x} and S_{4x}^3 [14] with which $\{I|\tau\}$ does not commute. Therefore, a new operation denoted by η is incorporated into the extended group when η represents the translation $\{E|\beta^{-1}\tau-\tau\}$ corresponding to the value -1. This process closes to form a complete group, the resulting group, G, now containing 32 elements. In G, $\{I|\tau\}^2=\eta^2=E$, and η commutes with all the elements, whereas

$$\{I|\tau\}\{\beta|0\}=\{\beta|0\}\{I|\tau\} \quad \text{or} \quad \{\beta|0\}\{I|\tau\}\eta,$$

according to whether the phase factor in (2) takes the value $+1$ or -1, respectively. Because of this noncommuting nature new representations arise that are different from those of D_{2d}. They are identified in Table I where representation matrices of some selected elements are given for all the X_j's pertinent to the present work.

[10] L. Kleinman and J. C. Phillips, Phys. Rev. **118**, 1153 (1960).
[11] For a review on this subject, see P. W. Anderson, *Concepts in Solids* (W. A. Benjamin, Inc., New York, 1963), p. 61.
[12] I. Goroff and L. Kleinman, Phys. Rev. **132**, 1080 (1963).
[13] C. Herring, J. Franklin Inst. **233**, 525 (1942). See another related paper, T. Sugita and E. Yamaka, Rept. Elec. Commun. Lab., Nippon Telegraph and Telephone Corp. (Japan) **2**, 24 (1954).
[14] G. F. Koster, in *Solid State Physics*, edited by F. Seitz and D. Turnbull (Academic Press Inc., New York, 1957), Vol. 5, p. 173. The notations of the group elements used in the present paper follow this article.

TABLE I. A unitary representation of some operations of the group $G^{\mathbf{k}}$, $\mathbf{k}=(2\pi/a)(1,0,0)$, for the diamond structure. The notations $\{C_{2y}|0\}$, $\{S_{4x}|0\}$ and $\{I|\tau\}$ are according to Koster. (See Ref. 14.) The last element η represents the primitive translation $\{E|\mathbf{t}\}$ for which $\exp(i\mathbf{k}\cdot\mathbf{t})=-1$.

	X_1		X_2		X_3		X_4	
	X_1	$\bar{X}_1$	X_2	$\bar{X}_2$	X_3	$\bar{X}_3$	X_4	$\bar{X}_4$
$\{C_{2y}\|0\}$	$\begin{pmatrix}0 & i\\ -i & 0\end{pmatrix}$		$\begin{pmatrix}0 & i\\ -i & 0\end{pmatrix}$		$\begin{pmatrix}0 & -i\\ i & 0\end{pmatrix}$		$\begin{pmatrix}0 & -i\\ i & 0\end{pmatrix}$	
$\{S_{4x}\|0\}$	$\begin{pmatrix}0 & i\\ -i & 0\end{pmatrix}$		$\begin{pmatrix}0 & -i\\ i & 0\end{pmatrix}$		$\begin{pmatrix}i & 0\\ 0 & -i\end{pmatrix}$		$\begin{pmatrix}-i & 0\\ 0 & i\end{pmatrix}$	
$\{I\|\tau\}$	$\begin{pmatrix}0 & 1\\ 1 & 0\end{pmatrix}$		$\begin{pmatrix}0 & 1\\ 1 & 0\end{pmatrix}$		$\begin{pmatrix}0 & 1\\ 1 & 0\end{pmatrix}$		$\begin{pmatrix}0 & 1\\ 1 & 0\end{pmatrix}$	
η	$\begin{pmatrix}-1 & 0\\ 0 & -1\end{pmatrix}$		$\begin{pmatrix}-1 & 0\\ 0 & -1\end{pmatrix}$		$\begin{pmatrix}-1 & 0\\ 0 & -1\end{pmatrix}$		$\begin{pmatrix}-1 & 0\\ 0 & -1\end{pmatrix}$	

First, we give a preliminary account concerning the compatibility relations and time reversal for subsequent discussions. In the representation X_1 in Table I two independent basis vectors denoted by X_1 and $\bar{X}_1$ are the limit of Δ_1 and $\Delta_{2'}$, respectively, when $\mathbf{k}$ approaches the X point along the Δ axis from the left. In the representations X_3 or X_4 which cannot split into different one-dimensional representations when going from X along the Δ axis, the most convenient choice will be the one by which each of two basis vectors has a direction of polarization along each of two orthogonal crystal axes, i.e., the $y[010]$ and $z[001]$ axes. For this purpose we choose appropriate linear combinations in the following way:

$$\langle\bar{X}_j|p_y|X_1\rangle=\langle X_j|p_z|X_1\rangle=0, \quad j=3,4, \tag{4}$$

where $\mathbf{p}$ is a polar-vector operator such as electron momentum. It can be shown that the representations X_3 and X_4 in Table I satisfy the above relations. The compatibility relations that are implied in Table I are therefore

$$\begin{gathered}\Delta_1\to X_1, \quad \Delta_{2'}\to\bar{X}_1: \quad \Delta_{1'}\to X_2, \quad \Delta_2\to\bar{X}_2;\\ \Delta_5{}^y\to X_3 \text{ or } X_4, \quad \Delta_5{}^z\to\bar{X}_3 \text{ or } \bar{X}_4,\\ \text{as} \quad k_x\to(2\pi/a)(1,0,0)-.\end{gathered} \tag{5}$$

Another point in writing IR as in Table I is the form of the inversion: The matrix for $\{I|\tau\}$ in Table I represents the equalities

$$\{I|\tau\}X_j=\bar{X}_j, \quad \{I|\tau\}\bar{X}_j=X_j, \tag{6}$$

which fix the relative phase of the two vectors X_j and $\bar{X}_j$. It is also convenient to choose the basis vectors such that every matrix element of momentum between them is a real quantity. This can be achieved, as a consequence of the connection between the operation $\{I|\tau\}$ and the time reversal, by requiring the following relations:

$$X_j{}^*=\{I|\tau\}X_j, \quad \bar{X}_j{}^*=\{I|\tau\}\bar{X}_j, \quad j=1,2,3,4. \tag{7}$$

All the above requirements fix the *phase* of the basis vectors of each IR, apart from a common factor ±1, in a unique form. We shall assume in the following that the phase conforms with Table I and Eq. (7), and discuss effects of elastic deformation on crystal wave functions as well as on energy bands near the X point.

It is customary to describe deformation of energy bands in terms of an elastic strain tensor $s_{\mu\nu}$ and a set of deformation potential operators, $D_{\mu\nu}(\mu,\nu=x,y,z)$,[15] in which one assumes one-electron-Hamiltonian perturbation approach. When it is applied in combination with symmetry analysis, one faces a problem concerning the difference between deformed and undeformed lattices or deformed and undeformed *reciprocal* lattices. Thus, in order for the perturbation theory to work consistently one scales a coordinate system in the deformed lattice so that it conforms with that in the undeformed lattice. Likewise, one scales a coordinate system in the deformed reciprocal lattice *contragrediently*. With this assumption one can discuss precisely the symmetry of the deformed structure in terms of that of the undeformed structure. Specifically, for the present purpose, the deformation potential operators are classified according to IR's of the group G under the assumption that the scaled coordinates are being taken. Thus, to first order in the conventional strains, $e_{\mu\nu}$ (see Ref. 2, hereafter referred to as H-F) the degenerate levels of each X_j may be modified as indicated by the following equation:

$$\begin{pmatrix}\epsilon_j{}^0 & \epsilon_j\\ \epsilon_j & \epsilon_j{}^0\end{pmatrix}\begin{pmatrix}\xi\\ \bar{\xi}\end{pmatrix}=\epsilon\begin{pmatrix}\xi\\ \bar{\xi}\end{pmatrix}, \tag{8}$$

where

$$\epsilon_j{}^0=\Xi_d(X_j)(e_{xx}+e_{yy}+e_{zz})+\Xi_u(X_j)e_{xx}, \tag{9}$$

$$\epsilon_j=\Xi_{u'}(X_j)e_{yz}, \tag{10}$$

in which $\Xi_d(X_j)$, $\Xi_u(X_j)$ and $\Xi_{u'}(X_j)$ are constants (deformation potential constants). The solutions of (8) are clearly $\epsilon=\epsilon_j{}^0\pm\epsilon_j$ for $\bar{\xi}=\pm\xi$: Namely, the one-electron level shifts by an amount $\epsilon_j{}^0$, and the twofold degeneracy is lifted with a splitting $2\epsilon_j$. It can be seen that an orthorhombic distortion by a yz-type stress is necessary for producing the level splitting.

Each eigenstate of such a split level is of the form

$$X_{jg}=(1/\sqrt{2})(X_j+\bar{X}_j) \quad \text{for} \quad \epsilon=\epsilon_j{}^0+\epsilon_j=\epsilon_j{}^0+\Xi_{u'}(X_j)e_{yz} \tag{11a}$$

and

$$X_{ju}=(1/\sqrt{2}i)(X_j-\bar{X}_j) \quad \text{for} \quad \epsilon=\epsilon_j{}^0-\epsilon_j=\epsilon_j{}^0-\Xi_{u'}(X_j)e_{yz}. \tag{11b}$$

These eigenstates can be characterized, in view of Table I or the relations in Eq. (6), by a *parity* with respect to the inversion operation $\{I|\tau\}$, since it is still allowed as a symmetry operation in the deformed crystal, when considered in the scaled coordinate. Therefore, *the symmetric eigenstate (11a) has the parity*

[15] G. D. Whitfield, Phys. Rev. **121**, 720 (1961).

+1, and the antisymmetric eigenstate (11b) has the parity −1 regarding the inversion operation $\{I|\tau\}$. This gives a definition of the sign of the deformation potential $\Xi_{u'}(X_j)$, and will be used later for interpreting our experimental results. To discuss the deformation effects on cyclotron resonance lines, the above considerations, confined to the X point, are extended to include dispersion of the one-electron energies with wave vector $\mathbf{k}$, i.e., the energy band, in the vicinity of the X point. The details are presented next.

B. Effect of Deformation on the Conduction Bands Δ_1 and $\Delta_{2'}$

In the absence of distortion, the two bands Δ_1 and $\Delta_{2'}$ intersect at the point X, i.e., $\mathbf{k}=(2\pi/a)(1,0,0)$. The tangents of the intersection are equal in magnitude but with opposite signs, because the following relation is shown to hold:

$$v_1=(1/m)\langle X_1|p_x|X_1\rangle=-(1/m)\langle\bar{X}_1|p_x|\bar{X}_1\rangle. \quad (12)$$

Here, p_x represents the electron momentum along the Δ axis, whose diagonal matrix element measures the tangent of the respective band. The equality (12) is a consequence of C_{2y} (rotation π about the [010] axis) so that the momentum p_x changes sign by this rotation while the bases X_1 and $\bar{X}_1$ transform according to IR given in Table I. The curvatures of both bands (the inverse effective mass) at the intersection point, on the other hand, are also equal since these relate only to the squares of the off-diagonal matrix elements of p_x. Therefore, either Δ_1 or $\Delta_{2'}$ may have a minimum on the Δ axis near the X point depending on the sign of the tangent, provided its magnitude is small. We shall put aside for the moment the question of the sign of the tangent but merely assume its magnitude to be small, which approximates the case for Si.[16] The minimum point, whose position we denote by k_0 (about $0.15\times 2\pi/a$ distant from X),[17] gives the conduction band edge where thermal electrons are populated. The energy-band ellipsoid centered at k_0 is then

$$E(\mathbf{k})=\frac{(k_x-k_0)^2}{2m_{\parallel}}+\frac{k_y^2+k_z^2}{2m_{\perp}}, \quad (13)$$

where units in which $\hbar=1$ are used. In the presence of orthorhombic distortion produced by a strain e_{yz} the crossing of the two bands will be resolved according to the argument given previously in Sec. IIA resulting in two separated bands, as indicated in Fig. 1. The ellipsoid in Eq. (13) under such a condition will be distorted to become[18]

$$E_e(\mathbf{k})=\delta_e+\frac{[k_x-k_0(e)]^2}{2m_{\parallel}(e)}+\frac{k_y^2+k_z^2}{2m_{\perp}(e)}+\alpha e_{yz}k_yk_z, \quad (14)$$

Here, δ_e represents a shift of the band edge, and the strain dependences of k_0 and the masses are explicitly indicated.

In our experiments the two masses $m_{\parallel}$ and $m_{\perp}$, their changes with strain to first order, and the additional parameter α in Eq. (14) can be measured accurately. In particular, the presence of the α term in Eq. (14) can be identified because of its anisotropic character which reflects the effect of lifting the band degeneracy at the X point. Its experimental identification may be aided, if advantage is taken of the following two theoretical predictions:

(1) The symmetry of the strain involved is the same as the one predicted in Sec. IIA, i.e., Eqs. (8) and (10): any strain of another symmetry cannot produce such a term.

(2) The magnitude of α is expected to be large compared to other strain-induced effective-mass shifts observable in resonances by virtue of the proximity of Δ_1 to $\Delta_{2'}$.

A precise theoretical expression for $m_{\parallel}$, $m_{\perp}$, and α may be established by making use of perturbation theory in second order for the undeformed and deformed lattices. The perturbation analysis is made at the band edge k_0 regarding the crystal momentum deviation as a perturbation expansion parameter (the $\mathbf{k}\cdot\mathbf{p}$ perturbation). For

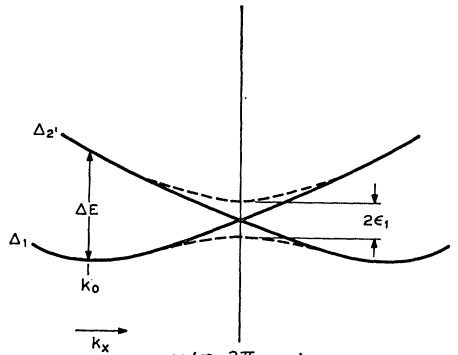

FIG. 1. Structure of the energy bands Δ_1 and $\Delta_{2'}$ near the crossing point X_1 at the zone boundary, $\mathbf{k}=(2\pi/a)(1,0,0)$, for a diamond lattice. The dotted lines indicate a splitting of the bands due to an orthorhombic deformation of the lattice. [See Eq. (17).]

[16] Kleinman and Phillips's results (Ref. 10) indicate $v_1>0$ so that the Δ_1 band is located lower than $\Delta_{2'}$ as shown in Fig. 1. Experimentally, there has been no evidence on this. One consideration based on spin-orbit effects can be made which favors $v_1>0$.

[17] G. Feher, Phys. Rev. 114, 1219 (1959).

[18] The ellipsoidal form in Eqs. (13) and (14) is unique. This can be understood from the fact that the group of $\mathbf{k}$ on the Δ axis consists of (1) E, C_{2x}, $2\sigma_d$, $2\sigma_v$, $2C_{4x}$ without distortion, and (2) E, C_{2x}, $2\sigma_d$ with the orthorhombic distortion e_{yz}. The allowance of the k_yk_z term in Eq. (14) is a consequence of the lack of the symmetry operations $2\sigma_v$ and $2C_{4x}$ in the latter case.

undeformed Si this gives[10]

$$\left(\frac{1}{m_{11}}\right)_{\Delta_1 k_0}=\frac{1}{m}+\frac{2}{m^2}\sum_l\frac{1}{E_{0l}}\langle\Delta_1|p_x|\Delta_1^{(l)}\rangle^2, \quad (15)$$

$$\left(\frac{1}{m_{\perp}}\right)_{\Delta_1 k_0}=\frac{1}{m}+\frac{2}{m^2}\sum_l\frac{1}{E_{0l}}\langle\Delta_1|p_y|\Delta_5^{y(l)}\rangle^2. \quad (16)$$

We note that similar formulas hold for the $\Delta_{2'}$ band. In these expressions the E_{0l} represent term differences between the conduction band and other relevant bands at the point k_0, and the matrix elements are those between the respective states at the same point.

A similar perturbation formula can be constructed for α. We defer this for a moment in order to estimate α in a conventional way using an expansion about X for the deformed band shape in terms of the tangents and curvatures of the unstrained bands. This can be done by solving a secular equation similar to Eq. (8):

$$\begin{bmatrix} v_1k_x & \epsilon_1+\frac{1}{m'}k_yk_z \\ \epsilon_1+\frac{1}{m'}k_yk_z & -v_1k_x \end{bmatrix}\begin{pmatrix}\xi\\ \xi\end{pmatrix}=\epsilon(\mathbf{k})\begin{pmatrix}\xi\\ \xi\end{pmatrix}. \quad (17)$$

(Hereafter, we take X to be the origin of the $\mathbf{k}$ vector.) Thus we can write α as a function of k_x as

$$\alpha(k_x)=\frac{2\Xi_{u'}(X_1)}{-\Delta E(k_x)}\frac{1}{m'}, \quad \Delta E(k_x)=2(v_1^2k_x^2+\epsilon_1^2)^{1/2}, \quad (18)$$

where v_1 is defined in Eq. (12) and ϵ_1 is the strain-splitting energy introduced in Eq. (10) for $j=1$ so that $\epsilon_1=\Xi_{u'}(X_1)e_{yz}$. To evaluate this for the conduction band minimum of silicon located at $k_x=k_0$, we note that $2|v_1k_0|$ gives the Δ_1-$\Delta_{2'}$ band separation (unstrained) which is $\sim$0.5 eV.[19] For attainable strains ϵ_1 will be of the order of millielectron volts, consequently $|v_1k_0|\gg\epsilon_1$. Therefore, if we tentatively assume $m'\approx m_{\perp}$ which will be considered more carefully later, we very roughly estimate the inverse mass shift αe_{yz} [the last term in Eq. (14)] to be $(1/m_{\perp})\times(\epsilon_1/|v_1k_0|)\sim(1/m)\times5\times10^{-2}$. This suggests that an anisotropic mass shift of several percent may be expected which is certainly measurable in our experiments.

For a more precise estimate we must set up a band-theoretical expression for α which takes into account the actual distance between the X point and the band-edge point, k_0. A way of treating such a problem has been indicated in several papers.[20] Essentially, one uses the $\mathbf{k}\cdot\mathbf{p}$ perturbation method modified by the presence of additional perturbing terms due to deformation. As mentioned previously, one is working with scaled coordinates to obtain a deformed energy band $\bar{E}_e(\mathbf{k})$ which has the same periodicity as the undeformed reciprocal lattice different from the deformed one. One therefore needs to restore the original coordinates in terms of the strain tensor $s_{\mu\nu}$ through the relation[21]

$$E_e(\mathbf{k})=\bar{E}_e((\mathbf{1}+\mathbf{s})\cdot\mathbf{k}), \quad (19)$$

where $E_e(\mathbf{k})$ represents the *true* energy band for the deformed lattice.

Performing these steps, we have derived the expression for α which is exact within one-particle band theory as follows:

$$\alpha=\frac{4\Xi_{u'}(k_0)}{-\Delta E}\frac{1}{m^2}\sum_l\frac{1}{E_{0l}}\langle\Delta_1|p_y|\Delta_5^{y(l)}\rangle \times\langle\Delta_5^{y(l)}|p_z|\Delta_{2'}\rangle-\frac{1}{m}\left(\left(\frac{m}{m_{\perp}}\right)_{\Delta_1 k_0}-1\right). \quad (20)$$

Here, the first term is a result of the combined perturbations of the $\mathbf{k}\cdot\mathbf{p}$'s and the deformation potentials $D_{\mu\nu}$'s to third order. We retain only those terms of perturbation which connect Δ_1 and $\Delta_{2'}$ through $D_{\mu\nu}$, as the energy interval ΔE between them at k_0 is an order of magnitude smaller than all the other E_{0l}'s involved in the perturbation terms. This term is represented by the ratio $\Xi_{u'}(k_0)/\Delta E$, where

$$\Xi_{u'}(k_0)=\langle\Delta_1|D_{yz}|\Delta_{2'}\rangle_{k_0}, \quad (21)$$

the only allowed matrix element of $D_{\mu\nu}$ between these two bands, is in the order of magnitude of several electron volts. The second term in (20) is the remaining contribution which results from the process of scaling and restoring the original coordinate system according to the above prescription.[21] This term is expected, however, to give only a small correction, inasmuch as the ratio $\Xi_{u'}(k_0)/\Delta E$ enhances the first term by a factor of 10 or so. It is clear now that only the first term is taken into account in the approximation used in Eq. (18) for which $\Delta E=2|v_1k_x|\gg\epsilon_1$. In our experiments the ratio $\Xi_{u'}(k_0)/\Delta E$ will be determined from the measured value of α and an appropriate estimate of the perturbation sum in (20).

Let us consider now in more detail the perturbation sums that appear in the expressions for the transverse

[19] The value of ΔE, the $\Delta_1-\Delta_{2'}$ (unstrained) band separation at k_0, has been estimated for Si to be 0.50±0.05 eV from the value 0.45 eV for the analogous gap in Ge calculated by M. L. Cohen (private communication). This value supercedes the earlier estimate of 0.35 eV by L. Liu, Phys. Rev. 126, 1317 (1962). We are indebted to J. C. Phillips for bringing this point to our attention.

[20] G. E. Pikus and G. L. Bir, Fiz. Tverd. Tela 1, 1642 (1959) [English transl.: Soviet Phys.—Solid State 1, 1502 (1960)]. Reference 15 and M. Nakayama, J. Phys. Soc. Japan (to be published).

[21] M. Nakayama (to be published).

mass (16) and α (20)

$$Z(k_x)=\frac{1}{2m}\sum_l \frac{1}{E_{0l}}\langle\Delta_1|p_y|\Delta_5{}^{y(l)}\rangle^2=\frac{1}{4}\left(\frac{m}{m_\perp}-1\right)_{k_x}, \quad (22)$$

$$Z'(k_x)=\frac{1}{2m}\sum_l \frac{1}{E_{0l}}\langle\Delta_1|p_y|\Delta_5{}^{y(l)}\rangle\langle\Delta_5{}^{y(l)}|p_z|\Delta_{2'}\rangle. \quad (23)$$

The perturbation sum $Z(k_0)$ for the effective mass $m_\perp$ of undeformed Si has been obtained by Kleinman and Phillips[10] from their calculations of Si energy bands by the OPW method. The calculations can also be extended to $Z'(k_0)$ for α, both results being given by[22]

$$Z(k_0)=1.07, \quad (24)$$

$$Z'(k_0)=-1.00. \quad (25)$$

Here we pass by the details of these calculations, which are summarized in Appendix A, and discuss some general points of the theory that underlie the above results.

The first question concerns the signs. While $Z(k_0)$ is known to have a positive sign ($m/m_\perp\sim 5$ from previous experiments), the sign of $Z'(k_0)$ is *a priori* uncertain. The sign of such a perturbation connecting different eigenstates has no absolute meaning but rather depends on the phase of the eigenfunctions. It is, however, related to how we have introduced the phase to define the sign of $\Xi_{w'}(k_0)$. To see the relation we take advantage of the closeness of k_0 to X, and replace $Z(k_x)$ and $Z'(k_x)$ by their limits as $k_x\to 0$ (the X point), where the symmetries of the wave functions are twofold greater than those for a general Δ point. From the compatibility relation (5) the representation Δ_5 continues either to X_3 or to X_4, the distinction resting on certain special properties of the representations allowed only at the X point. The difference is exemplified by the IR's for S_{4x} (rotation $\pi/2$ about the [100] axis followed by the reflection through the (100) plane) listed in Table I, which lead to the following two relations:

$$\langle X_1|p_y|X_3\rangle=\langle\bar{X}_1|p_z|X_3\rangle, \quad (26a)$$

$$\langle X_1|p_y|X_4\rangle=-\langle\bar{X}_1|p_z|X_4\rangle. \quad (26b)$$

Therefore, we can write

$$Z(X)=\frac{1}{2m}\sum_l \frac{1}{E_{0l}}\langle X_1|p_y|X_3{}^{(l)}\rangle^2 + \frac{1}{2m}\sum_l \frac{1}{E_{0l}}\langle X_1|p_y|X_4{}^{(l)}\rangle^2 \quad (27a)$$

and

$$Z'(X)=\frac{1}{2m}\sum_l \frac{1}{E_{0l}}\langle X_1|p_y|X_3{}^{(l)}\rangle^2 - \frac{1}{2m}\sum_l \frac{1}{E_{0l}}\langle X_1|p_y|X_4{}^{(l)}\rangle^2. \quad (27b)$$

Combining these equations we see

$$Z'(X)=-Z(X)+\frac{1}{m}\sum_l \frac{1}{E_{0l}}\langle X_1|p_y|X_3{}^{(l)}\rangle^2, \quad (28)$$

so [recalling that $Z(X)>0$] the problem of sign of $Z'(X)$ reduces essentially to the relative ordering of the one-electron levels $X_3{}^{(l)}$. In Table II results from the current band theory for the X point in Si are listed in order of increasing energy. Clearly, the only positive contribution to $Z'(X)$ comes from the $2p$-core X_3 state, which, however, is entirely negligible in view of the large energy denominator and small matrix element for this term. In fact, numerical calculations show that more than 95% of the sums in Eqs. (27a) and (27b) come from the single valence X_4 level from which the results in Eqs. (24) and (25) are deduced with some additional corrections due to the difference between k_0 and X as well as other minor corrections. It should be emphasized that the conclusion $Z'<0$ cannot be affected by the detailed structure of the conduction bands above X_1 or the fact that the foregoing arguments were constructed at X rather than k_0.

In the above connection another question concerns the theoretical accuracy. Although considerable progress has been made in the band theory of valence semiconductors especially for Si, actual computations are still in an incomplete state. Perhaps one of the most serious problems is the uncertainty of the exchange potential which yields numerical ambiguities sometimes of order of an eV for calculated term values and, thus, for the energy denominators in the perturbation formulas. Fortunately, for the present purpose the important term difference $E(X_{1\,\mathrm{cond}})-E(X_{4\,\mathrm{val}})$ is known experimentally. There remains, however, some uncertainty in the value of the energy gap $E(\Delta_1)-E(\Delta_5)$ at k_0 which is expected to be about 5% smaller than the gap at X. (See Ref. 22.) Another source of inaccuracy is the core-core contribution to momentum matrix elements in the use of the OPW functions (oscillatory part). In general,

TABLE II. One-electron energy levels in Ry at X after Kleinman and Phillips (Ref. 10) (with k-independent exchange potential). The conduction band Δ_1 continues to the second valence X_1 level denoted by $X_1{}^{(2)}$. For comparison the measured term difference $E(X_1{}^{(2)})-E(X_4)$ is 0.32 Ry (Ref. 22).

1s-Core	2s-Core	2p-Core	Valence			
X_1	X_1	X_1, X_3, X_4	$X_1{}^{(1)}$	X_4	$X_1{}^{(2)}$	$X_3\cdots$
−131.4	−12.0	−8.72	−2.01	−1.77	−1.38	∼0.4

[22] These values are based on the term difference $E(\Delta_1)-E(\Delta_5)=4.1$ eV at k_0 estimated from the experimentally determined energy gap at X of $E(X_1)-E(X_4)=4.3$ eV. For the latter value see D. Brust, Phys. Rev. **134A**, 1337 (1964). It is interesting to note that the result for $Z(k_0)$ so obtained predicts [see Eq. (22)] an effective mass, $m_\perp/m=0.19$ in good agreement with the experimental value [Eq. (31)].

however, momentum matrix elements are more reliable than term differences.[23]

In view of these facts we shall not use the value of Eq. (25) directly to deduce $\Xi_{u'}(k_0)/\Delta E$. Instead, we use the theoretical value of the ratio

$$f=Z'(k_0)/Z(k_0)=-0.94\pm0.02 \qquad (29)$$

in combination with a value for $Z(k_0)$ derived from measurements of $m_\perp$. It is expected that the estimate (29) is more reliable than those in (24) and (25), because by taking the ratio the inaccuracy of the term difference $E(\Delta_1)-E(\Delta_5)$ can be eliminated and absorbed in the experimental quantity $m_\perp$. Furthermore, the uncertainty in the matrix elements themselves will be largely canceled out. Thus, the uncertainty quoted in Eq. (29) is shown to arise mainly from the first-order correction of the momentum matrix elements involved in Z and Z' due to the difference between k_0 and X (see Appendix A).

In summary, then, we see that the above result for f permits us to evaluate the band-mixing ratio $\Xi_{u'}/\Delta E$ of Eq. (20) from the experimental values for $m_\perp$ and α. This will be carried out explicitly in Sec. IVB.

III. EXPERIMENTAL DETAILS

The experimental apparatus and techniques used here are the same as described previously in (H-F).[2] The cyclotron resonance measurements were made at 1.26°K on a superheterodyne X band (~8900Mc/sec) microwave spectrometer. The magnetic field strength was measured by proton nuclear magnetic resonance. The microwave frequency was monitored by heterodyning techniques using an HP 540A transfer oscillator—HP 524 frequency counter combination. Under the optimum conditions—the microwave power held to low levels ($\sim10^{-8}$ W) and the intensity of the (white) light for carrier production minimized using "grey" filters—the electron linewidths were characterized by $\omega\tau\sim160$. The samples [the same as used in (H-F)] were cut from a single crystal of 5000Ω cm p-type silicon, whose dimensions were approximately 7×3.5×0.7 mm. Before each measurement the crystallographic orientation of the mounted samples was checked by noting the symmetry of the electron cyclotron resonance lines as the direction of the magnetic field was changed.

The resonance signals were observed and their line shifts with strain were measured for the electrons of all six "valleys" (the [100] and its equivalent directions). The strain apparatus, the perpendicular squeezor, has been described earlier[2] in detail. Table III shows the strain-stress relations reproduced from (H-F),[2] which are also pertinent here for the present experimental arrangements. The strain was applied to the sample by compressing the two halves of a split TE_{101} rectangular cavity. A force was thus transmitted to the sample which lay inside just above the cavity bottom (near maximum H_1 field). The compression was controlled by a spring balance external to the cryostat permitting a working range of stresses from 0 to 2500 kg/cm². Thus, the geometry was such that the direction of the stress was perpendicular to both the Dewar axis and the microwave electric field. The Varian magnet rotating about the Dewar axis could reach all directions from $H_0\|T$ to $H_0\perp T$. The orientation of the uniaxial stress was determined from the symmetry of the split-band hole line. In all cases the stress axis coincided with the desired principal crystallographic direction to within 1°. It was found that as the stress was applied the sample sometimes shifted by perhaps <0.1°, which is small but sufficient to cause considerable inaccuracy if the effective mass depends strongly on angle. Most of the measurements, therefore, were made with H_0 either parallel or perpendicular to the major axis of the electron ellipsoid, for which the cyclotron effective masses are extrema.

It is predicted from Table IV that the band-mixing

TABLE III. The "conventional" strain components [see (H-F)] for orientations of stress along each of the three principal crystallographic axes. The cubic compliance constants for silicon are $s_{11}=7.48\times10^{-7}$ cm²/kg, $s_{12}=-2.10\times10^{-7}$ cm²/kg, and $s_{44}=12.24\times10^{-7}$ cm²/kg at 0°K.

$T\|\|[100]$	$T\|\|[011]$	$T\|\|[111]$
$e_{xx}=s_{11}T$	$e_{xx}=s_{12}T$	$e_{xx}=e_{yy}=e_{zz}=(s_{11}+s_{12})(T/3)$
$e_{yy}=e_{zz}=s_{12}T$	$e_{yy}=e_{zz}=(s_{11}+s_{12})(T/2)$	$e_{xy}=e_{xz}=e_{yz}=s_{44}(T/3)$
$e_{xy}=e_{xz}=e_{yz}=0$	$e_{xy}=e_{xz}=0$	
	$e_{yz}=s_{44}(T/2)$	

TABLE IV. The shifts, $\Delta m^*/m^*$, of the cyclotron-resonance effective mass calculated from Eq. (14) in the text for $T\|\|[100]$, $T\|\|[011]$, and $T\|\|[111]$. The directions chosen for the magnetic field, H_0, correspond to the present experimental situations shown in Fig. 2. Corrections due to other small effects discussed in the text are not included.

Direction of magnetic field, H_0	$T\|\|[100]$ Any	$T\|\|[011]$ (100) Plane	$T\|\|[111]$ (011 Plane)	
[100] ellipsoids	0	$\frac{m_\perp}{2}\alpha e_{yz}\cos2\varphi$	0	$H_0\|\|[100]$
			$\frac{m_\perp^2}{m_\parallel+2m_\perp}\alpha e_{yz}$	$H_0\|\|[111]$
			$\frac{m_\perp}{2}\alpha e_{yz}$	$H_0\|\|[011]$
[010] [001] ellipsoids	0	0	0	$H_0\|\|[100]$
			$\frac{m_\perp^2}{m_\parallel+2m_\perp}\alpha e_{yz}$	$H_0\|\|[111]$
			0	$H_0\|\|[011]$

[23] J. C. Phillips, Phys. Rev. **125**, 1931 (1962). See also J. C. Phillips, D. Brust, and F. Bassani, in *Proceedings of the International Conference on the Physics of Semiconductors, Exeter, 1962.* (The Institute of Physics and the Physical Society, London, 1962), p. 564.

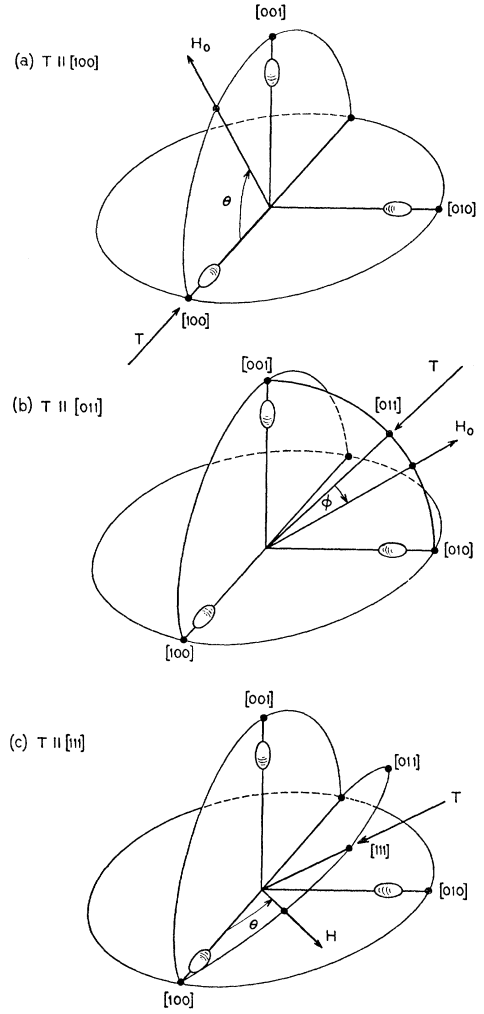

FIG. 2. Schematic representation of the geometries used in the stress experiments. The three cases studied are: (a) $T\|[100]$, (b) $T\|[0\bar{1}1]$, and (c) $T\|[111]$. For these three situations the magnetic field, H_0 is rotated as shown in the (010), (100), and (0$\bar{1}$1) planes, respectively, with the angles of H_0 measured, respectively, from the [100], [011], and [100] axes.

parameter α introduced in Sec. IIB can be best determined by observing the line shift of the [100] valley resonance under the particular experimental arrangement, $T\|[011]$ and $H_0\perp[100]$. For the sake of completeness, however, measurements for $T\|[100]$ and $T\|[111]$ were also made. These geometries are all depicted in Fig. 2. Inasmuch as the electron effective mass *shifts* are extrema for $T\|[100]$ and $T\|[011]$, misorientations of stress as small as 1° are expected to have a negligible effect (<1 part in 10^3) on the measurements. For $T\|[111]$, however, the effective-mass shifts depend upon the stress direction to first order so even small misorientations can contribute substantial errors. In the former two conditions, i.e., $T\|[100]$ and $T\|[011]$, marked change in the relative intensities of the different valley resonances are observed which result from valley splitting: Each band edge shifts by an amount δ_e indicated in Eq. (14), which is different for valleys differently situated with respect to the stress.[24] For $T\|[011]$ the intensity of the [100] valley resonance from which α is to be determined decreases with increasing compression T, showing that this is an ascending ellipsoid.[25] It was found that accurate measurement for this ellipsoid is possible only if the microwave electric field E_1 is applied in directions perpendicular to the major axis of the ellipsoid, i.e., the direction for which the signal intensity is optimized.

IV. EXPERIMENTAL RESULTS

A. Electron Effective Mass

Early in the course of the present work it became apparent that the values of the electron-effective mass (for $T=0$) disagreed considerably with the results of some of the earlier measurements. This disagreement has been noted previously.[26,27] Since the sharpness of the electron lines here ($\omega\tau\sim160$) has made possible a measurement of the effective masses to an accuracy substantially greater than given hitherto, it seemed worthwhile to include these results.

Determinations of the two components $m_{\|}$ and $m_{\perp}$ were made from an over-all fit of the anisotropy of the cyclotron mass m^*, assuring exact orientation of the magnetic field direction with respect to the crystal axes. Figure 3 shows such a fit for H_0 in the (0$\bar{1}$1) plane with a set of values

$$m_{\|}/m=0.9163\pm0.0004, \tag{30}$$

$$m_{\perp}/m=0.1905\pm0.0001. \tag{31}$$

The uncertainties represent the maximum deviation from the quoted average values from a number of independent runs. The small deviations from run to run are believed to be due primarily to uncertainties of the order of 0.1° in determining the sample orientation after it has been mounted in the cryostat. Measurements were also made at 54 kMc/sec (5.6 mm), the results of which coincide with the X band values in (30) and (31).

The electron effective masses in Eqs. (30) and (31) are overlapped by the previous values $m_{\perp}/m=0.192\pm0.001$ and $m_{\|}/m=0.90\pm0.02$ obtained by Rauch *et al.*[26] at 2.1 mm and $m_{\perp}/m=0.19$ and $m_{\|}/m=0.92$

[24] In principle, one ought to be able to determine the value of the deformation potential Ξ_u [see Eq. (9) in Sec. IIA] by measuring the relative amplitudes of the electron resonances with uniaxial stress applied [see A. C. Rose-Innes, Proc. Phys. Soc. (London) **72**, 514 (1958)]. However, the results in silicon [J. C. Hensel and G. Feher (unpublished)] seem to be seriously at odds with values obtained by other techniques, the difficulty perhaps being due to the light generated carriers not achieving thermal equilibrium before recombination.

[25] This is consistent with Wilson-Feher's result (Ref. 5) indicating that $\Xi_u>0$.

[26] G. J. Rauch, J. J. Stickler, G. S. Heller, and H. J. Zeiger, Phys. Rev. Letters 4, 64 (1960).

[27] D. M. S. Bagguley, R. A. Stradling, and J. J. Whiting, Proc. Royal Soc. (London) A262, 365 (1961).

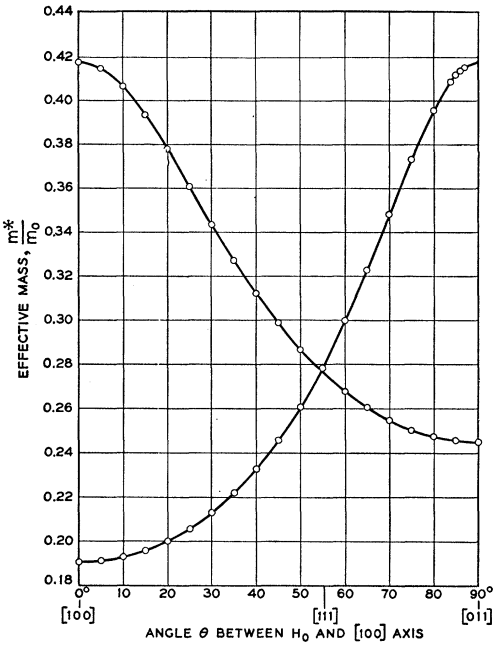

FIG. 3. Anisotropy of the cyclotron resonance effective mass for electrons in unstrained silicon. The magnetic field, H_0 is rotated in the (01$\bar{1}$) plane and the angles are measured from the (100) axis [see Fig. 2c)]. The curves were calculated for ellipsoidal energy surfaces using the effective-mass values; $m_\perp=0.1905m$ and $m_{II}=0.9163m$.

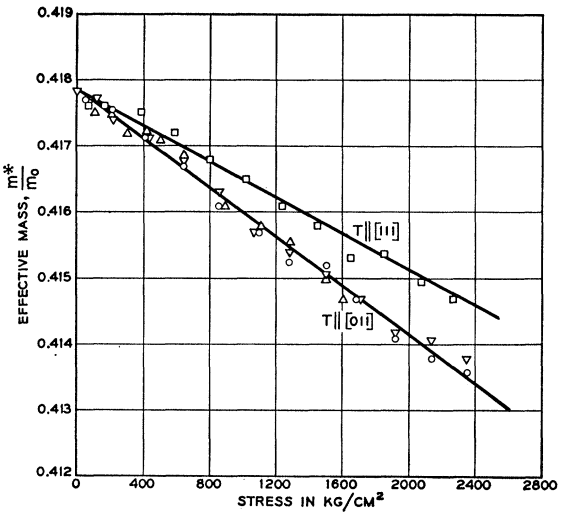

FIG. 4. Dependence of the electron effective mass ($H_0\|[011]$) for the (001) ellipsoid on a uniaxial stress applied in turn to the [001] and [111] axes. In reference to Fig. 2 these measurements correspond, respectively, to case (b) with $\varphi=0°$ and case (c) with $\theta=90°$. The zero-stress effective mass is $(m_\perp m_{II})^{1/2}=(0.4178\pm0.0002)m$.

obtained by Bagguley *et al.*[27] at 8.8 mm. There is, however, a significant disagreement with the values of the longitudinal mass $m_{II}/m\sim0.97$ obtained in the early measurements[28] at X and K band. The reason for the high values of m_{II} in the old measurements is at present not understood.[29]

B. Mass Shifts Due to Uniaxial Stress

Table III indicates that in each orientation of stress there always appear strain components of the type e_{xx}, e_{yy}, e_{zz} which cause "symmetry preserving" shifts

$$m_{II}(e)=m_{II}+\Delta m_{II}, \quad m_\perp(e)=m_\perp+\Delta m_\perp. \tag{32}$$

In addition, for $T\|[111]$ off-diagonal strain components may also give rise to small terms of the type $\alpha'(e_{xy}k_xk_y+e_{xz}k_xk_z)$ which must be included in the expression (14) for the [100] ellipsoid. Experimentally, both of these secondary shifts must be separated from that due to Δ_1-$\Delta_{2'}$ mixing in order to determine the parameter, α.

Figure 4 shows the observed stress dependence of the cyclotron effective mass of the [100] ellipsoid under the two conditions T, $H_0\|[011]$ and $T\|[111]$, $H_0\|[011]$. Under the same conditions the other ellipsoids [010] and [001] exhibited a shift which was at least an order of magnitude smaller than that of the [100] ellipsoids. For $T\|[011]$, the anisotropy of the [100] ellipsoid line was measured varying the angle φ of H_0 [see Fig. 2(b)] at a fixed value of stress. From Fig. 5 we thus obtain

$$\Delta m^*/m^*=a+b\cos2\varphi. \tag{33}$$

where

$$a=1.4\times10^{-3}, \quad b=-(9.1\pm0.4)\times10^{-3}, \tag{34}$$

for $T=1800$ kg/cm².

This angular variation coincides with that predicted in Table IV. The anisotropic shift b is considerably larger than the isotropic shift a, indicating the presence of the expected mixing parameter α. This view was further checked by several supplementary measurements as follows:

(1) $T\|[100]$

(a) [100] (descending) ellipsoid: $(\Delta m_{II}/m_{II})\sim-1\times10^{-3}$.

(b) [010] and [001] (ascending) ellipsoids:

$(\Delta m_{II}/m)\sim(\Delta m_\perp/m)\sim+1\times10^{-3}$ for $T=2500$ kg/cm². No mass shifts other than these were detected; in particular, there was no change in the axial symmetry of

[28] From the early cyclotron resonance measurements in silicon the effective mass values reported were $m_\perp/m_0=0.19\pm0.01$ and $m_{II}/m_0=0.97\pm0.02$ [G. Dresselhaus, A. F. Kip, and C. Kittel, Phys. Rev. **98**, 368 (1955)], and $m_\perp/m_0=0.19\pm0.01$ and $m_{II}/m_0=0.98\pm0.04$ [R. N. Dexter, H. J. Zeiger, and B. Lax, Phys. Rev. **104**, 637 (1956)].

[29] The possibility has occurred to us that the high values of m_{II} in the early measurements may have resulted from the effects of strain. However, for several reasons this appears unlikely. From considerations of the geometries of these experiments one cannot, from the vantage point of the present work, account for either the sign of the shift or its magnitude. Furthermore, a uniaxial stress of sufficient magnitude to shift the electron mass significantly would certainly have decoupled the valence bands and, thus, prevented observation of the usual "light" and "heavy" hole resonances.

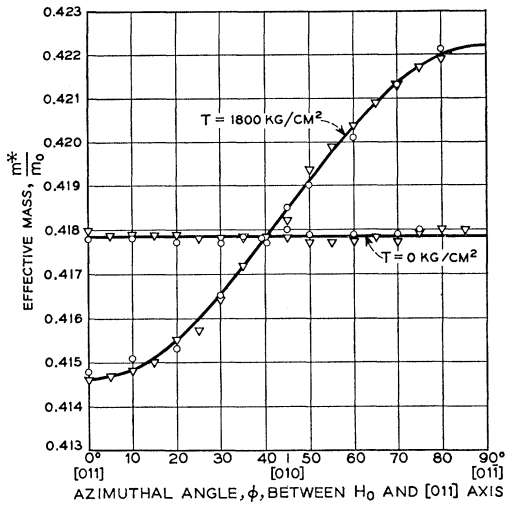

FIG. 5. The anisotropy of the cyclotron resonance effective mass of the (100) ellipsoid for zero stress and for $T\|[011]$ ($T=1800$ kg/cm^2). The magnetic field, H_0 is rotated in the (100) plane [see Fig. 2(b)] by angle φ measured from the (011) axis. For zero stress the anisotropy vanishes by virtue of the axial symmetry of the ellipsoid about the [100] axis. For $T=1800$ kg/cm^2 the anisotropy is fitted by a curve derived from the equation $\Delta m^*/m = a+b\cos\varphi$, where $a=1.4\times10^{-3}$ and $b=-(9.1\pm0.4)\times10^{-3}$.

the [010] (and [001]) ellipsoid. The symmetry was checked by measuring the cyclotron effective mass, $m^*=(m_{\|}m_{\perp})^{1/2}$, for the [010] ellipsoid as H_0 was rotated in the (010) plane. The effective mass was found to be constant to $\sim10^{-4}$.

(2) $T\|[011]$

The anisotropic shift of Eqs. (33) and (34) was obtained only for the [100] (ascending) ellipsoid: The [010] and [001] (descending) ellipsoids exhibited $(\Delta m_{\perp}/m)\sim(\Delta m_{\|}/m)\sim-1\times10^{-3}$ for $T=2500$ kg/cm^2 with no angular variation.

(3) $T\|[111]$

In this case, all valleys are equivalent with respect to the stress direction, and no relative changes of intensities are expected. The difference between the two types of ellipsoids, [100] and [010] (or [001]), arises only with regard to the direction of H_0.

(a) $H_0\|[100]$: $|\Delta m^*/m^*|<10^{-3}$ for both types of ellipsoids.

(b) $H_0\|[011]$: The [100] Ellipsoid exhibited a decrease of m^* with increasing stress. This is shown in Fig. 4 in comparison with the case $T\|[011]$. From Table IV the ratio of the shifts for these two cases are expected to involve only the ratio of the respective strains:

$$\frac{\Delta m^*(T\|[111])}{\Delta m^*(T\|[011])}=\frac{e_{yz}(111)}{e_{yz}(011)}=\frac{2}{3}. \tag{35}$$

The two linear shifts in Fig. 4 are seen to be in qualitative accord with this ratio. When the mass shifts are corrected by extracting the isotropic parts, we find

$$\left.\frac{\Delta m^*(T\|[111])}{\Delta m^*(T\|[011])}\right|_{\text{exp}}=0.63\pm0.05 \tag{36}$$

in good agreement with Eq. (35).

(c) $H_0\|[111]$: A sizeable decrease in effective mass for all ellipsoids with increasing stress was observed. This geometry is the one that might have revealed the second anisotropic term $\alpha'(e_{xy}k_xk_y+e_{xz}k_xk_z)$. This was not observed, however, since the cyclotron effective mass was not an extremum for $H_0\|[111]$ which made the measurements inaccurate.

It is concluded from all the above-stated results, first, that the expected anisotropic shift due to Δ_1-$\Delta_{2'}$ band mixing is verified indicating the correctness of the model (14), and second, that this is essentially the only significant mass shift in the measurements.

The measured anisotropic shift b in Eq. (34) corresponds to a value of α as follows:

$$\alpha=-\frac{(9.1\pm0.4)\times10^{-3}}{(m_{\perp}/m)(m/2)e_{yz}}=\frac{86.8\pm5.0}{m}. \tag{37}$$

The uncertainties in this number reflect mainly the estimated uncertainties (approximately 5%) involved in determining the magnitude of the stress, T from which the strain e_{yz} is calculated. From the argument in Sec. IIB [Eqs. (20), (22), (23), (29)] the band-mixing ratio $\Xi_{u'}(k_0)/\Delta E$ is expressed in the form

$$\frac{\Xi_{u'}(k_0)}{-\Delta E}=\frac{1}{2f}\left(1+\frac{m\alpha}{(m/m_{\perp})-1}\right), \tag{38}$$

where f is given by Eq. (29). Inserting the measured values of $m_{\perp}$ and α [Eqs. (31) and (37), respectively] and using the theoretical value of f, we obtain

$$\Xi_{u'}(k_0)/\Delta E=11.4\pm1.1, \tag{39}$$

where the quoted uncertainty now includes both the experimental and theoretical ones. Also, the OPW calculations provide an estimate $\Delta E=0.50$ eV[19] from which

$$\Xi_{u'}(k_0)\approx 5.7\text{ eV}. \tag{40}$$

For this result an uncertainty is difficult to assign but a value of ±1 eV may not be unreasonable.

V. DISCUSSION

A. Interpretation of the Sign of $\Xi_{u'}$

Our result that the deformation potential $\Xi_{u'}(k_0)$ is positive depends of course upon our initial choice of the relative phase of the Δ_1 and $\Delta_{2'}$ functions at k_0 and by itself has no absolute meaning. Nevertheless, the procedure we adopted so far to characterize the sign should

yield a physically significant conclusion which is invariant under alterations of the phases. Here we seek such an interpretation. For this purpose, let us consider the $\lim k_0 \to 0$, i.e., the X point, where the effect of e_{yz}-type strain produces a decoupling of the degenerate bands, and recall the result of Sec. IIA concerning the *parity* of the corresponding eigenfunctions. There, we have defined the sign of $\Xi_{u'}(X_1)$ such that the symmetric combination $X_1+\bar{X}_1$ whose parity regarding the operation $\{I|\tau\}$ is *even*, has a perturbation energy $\epsilon_1=\Xi_{u'}(X_1)e_{yz}$ and that the antisymmetric combination $X_1-\bar{X}_1$ whose parity regarding $\{I|\tau\}$ is *odd* has an energy $-\epsilon_1=-\Xi_{u'}(X_1)e_{yz}$. The positive sign of $\Xi_{u'}$ with a negative strain e_{yz} implies, therefore, that the even eigenstate has a lower perturbation energy than the odd eigenstate. We assume that because of the proximity of the band edge k_0 to X, the matrix element $\Xi_{u'}(k_x)$ varies for $k_0 \leq k_x \leq (2\pi/a)(1,0,0)$ only slightly without sign change, which is, indeed, the case for the effective-mass perturbation sum. We can summarize the foregoing in the following statement:

The splitting of the doubly degenerate X_1 states of the conduction band in Si by an orthorhombic distortion is such, that under a uniaxial compression of the crystal along the twofold axis [011] one of the split eigenstates with an even parity has a lower energy than the other eigenstate with an odd parity with respect to an interchange of the two atoms (0,0,0) and $\tau=(a/4, a/4, a/4)$ in the unit cell.

Such a property must certainly be connected with some nature of covalent bonds of electrons in the crystal, the understanding of which requires more explicit presentation of valence-electron orbitals. In the spirit of the OPW method as well as the tight-binding theory[20] one can write the two basis function X_1 and $\bar{X}_1$ in a form

$$X_1=X_1^s\cos\vartheta+X_1^p\sin\vartheta,\ \bar{X}_1=\bar{X}_1^s\cos\vartheta+\bar{X}_1^p\sin\vartheta, \quad (41)$$

where the superscripts s and p indicate atomic "s-like" and "p-like" functions. More precisely

$$\begin{aligned} &X_1^s(r)=C_s[s(r)+is(\mathbf{r}-\tau)],\\ &X_1^p(r)=C_p[x(\mathbf{r})+ix(\mathbf{r}-\tau)], \quad (42)\\ &\bar{X}_1^s(\mathbf{r})=\text{c.c. of } X_1^s,\ \bar{X}_1^p(\mathbf{r})=\text{c.c. of } X_1^p. \end{aligned}$$

Here we do not mean to imply that these are the Bloch sums of pure atomic functions. The OPW functions can also be shown under certain restrictions to allow such a representation. For the present, $s(\mathbf{r})$ and $x(\mathbf{r})$ are defined only as satisfying

$$s(-\mathbf{r})=s(\mathbf{r}),\quad x(-\mathbf{r})=-x(\mathbf{r}) \quad (43)$$

in addition to the translation and the point symmetries. In this sense, these resemble atomic s- and p_x-like orbitals, respectively, just in the vicinity of the Si nucleus. The constants C_s and C_p must be suitably chosen so that $X_1(r)$ (a) is normalized (e.g., in the unit cell), and (b) satisfies the reality conditions (7).

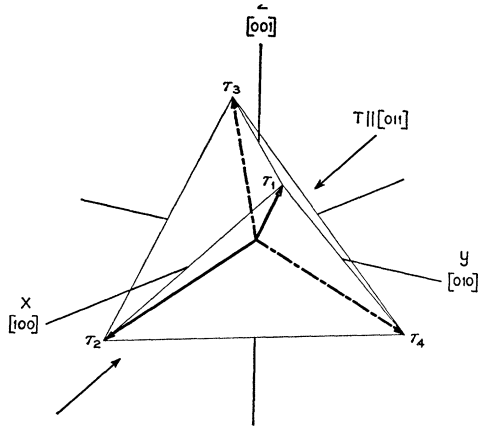

FIG. 6. A unit tetrahedron in the diamond structure. Four bonds connecting the center atom and the vertex atoms are indicated by bond straight lines and dotted lines. These two types of bonds have projections on the (100) plane parallel and perpendicular to the external uniaxial stress applied along the [011] direction, so that their response to the stress can be different.

Invoking the relations

$$\begin{aligned} &\{I|\tau\}s(\mathbf{r})=s(-\mathbf{r}+\tau)=s(\mathbf{r}-\tau),\\ &\{I|\tau\}x(\mathbf{r})=x(-\mathbf{r}+\tau)=-x(\mathbf{r}-\tau), \end{aligned}$$

we can see that the reality conditions (7) are satisfied by the choice

$$C_s=N_s e^{-i(\pi/4)},\quad C_p=N_p e^{i(\pi/4)}, \quad (44)$$

where N_s and N_p are real and assumed to be positive.

The split eigenfunctions are now given in a form such that their parity with respect to the operation $\{I|\tau\}$ is clearly evident

$$\begin{aligned} X_{1g}=\frac{1}{\sqrt{2}}(X_1+\bar{X}_1)&=(s(\mathbf{r})+s(\mathbf{r}-\tau))N_s\cos\vartheta\\ &+(x(\mathbf{r})-x(\mathbf{r}-\tau))N_p\sin\vartheta, \quad (45a)\\ X_{1u}=\frac{1}{\sqrt{2i}}(X_1-\bar{X}_1)&=-((s(\mathbf{r})-s(\mathbf{r}-\tau))N_s\cos\vartheta\\ &+(x(\mathbf{r})+x(\mathbf{r}-\tau))N_p\sin\vartheta. \quad (45b) \end{aligned}$$

Thus, the even (X_{1g}) and odd (X_{1u}) parity eigenfunctions are essentially the *bonding* and *antibonding* orbitals, respectively, regarding the two nearest neighbor atoms in the unit cell both for s and p_x functions, as would be expected. It is, however, important to note that the concepts of the "bonding" and "antibonding" are to be reversed when one considers a pair of nearest-neighbor atoms in certain *other* directions. It can be visualized most easily by looking at a unit tetrahedron (Fig. 6). For the atom located at the origin the four nearest neighbor atoms at the vertices

$$\tau_1=a(\tfrac{1}{4},\tfrac{1}{4},\tfrac{1}{4}),\ \tau_2=a(\tfrac{1}{4},-\tfrac{1}{4},-\tfrac{1}{4}),\ \tau_3=a(-\tfrac{1}{4},-\tfrac{1}{4},\tfrac{1}{4}),$$

and

$$\tau_4=a(-\tfrac{1}{4},\tfrac{1}{4},-\tfrac{1}{4})$$

are grouped, regarding the symmetry operations for $X(\mathbf{k}=(2\pi/a)(1,0,0))$, into two sets: the first two atoms whose coordinate vectors τ_1, τ_2 have projections on the (100) plane (yz plane) parallel to the [011] direction, and the second two atoms whose coordinate vectors τ_3, τ_4 have projections parallel to the [0$\bar{1}$1] direction. The bonding orbital, $X_1+\bar{X}_1$ regarding the pair of atoms connected by the vector τ_1 or τ_2 is in fact an "antibonding orbital" regarding the pair connected by τ_3 or τ_4, and vice versa. In a group-theoretical terminology introduced in Sec. IIA, this distinction is expressed through the relation

$$\{I|\bar{\tau}\}=\{I|\tau\}\eta, \text{ where } \tau \text{ represents } \tau_1 \text{ or } \tau_2 \text{ and } \bar{\tau} \text{ represents } \tau_3 \text{ or } \tau_4. \quad (46)$$

Since the irreducible representations of $\{I|\tau\}$ and $\{I|\tau\}\eta$ are different just in sign (from the argument of Sec. IIA), the stated reversal of the bonding and antibonding natures follows from the relations

$$\{I|\tau\}X_{1g}=X_{1g}, \quad \{I|\tau\}X_{1u}=-X_{1u}, \quad (47a)$$

$$\{I|\bar{\tau}\}X_{1g}=-X_{1g}, \quad \{I|\bar{\tau}\}X_{1u}=X_{1u}. \quad (47b)$$

In the absence of orthorhombic distortions of a unit tetrahedron there is nothing to distinguish any one of four bonds from the others, which is just the reason for the double degeneracy of the X_1 states. In the sense of Bloch sums [linear combination of atomic orbitals (LCAO)], as a consequence, two s-like orbitals or two p-like orbitals centered at two neighboring nuclei cannot be hybridized.[30] [On the other hand, an "s-p hybridization" does occur between the two neighboring atoms, as is expressed by the factors $\cos\vartheta$, and $\sin\vartheta$ in (41).] When the tetrahedron is squeezed along either one of the twofold axes [011] and [0$\bar{1}$1] which are perpendicular to the [100] axis, the two types of bonds become distinct: The one is *parallel* and the other is *perpendicular* to the direction of squeeze, when projected on the (100) plane. Under these circumstances the two similar orbitals centered at the neighboring nuclei will be hybridized to form bonding and antibonding orbitals, the double degeneracy being now lifted so that one type of bond favors the applied distortion more than the other.

From this consideration we now arrive at our final interpretation of the experimental result: When a unit tetrahedron in Si crystal is compressed along a twofold symmetry axis, the four bonds connecting the center atom and the vertex atoms, which are otherwise equivalent, become distinct. The (conduction-) electron state corresponding to the bonding orbitals of those bonds which have components parallel to the direction of compression (and hence which tend to become shorter by the compression) has a lower energy than the state corresponding to the bonding orbitals of those bonds having no parallel components.

The distinction between the two types of bonds under orthorhombic distortions has indeed been observed, though indirectly, in the cyclotron-resonance line shift under the condition $T\|[011]$, when the dc field is rotated from the [011] to the [0$\bar{1}$1] direction (Fig. 5).

B. The Covalent Bonds in Terms of the OPW Theory

With the aid of the OPW calculations of Kleinman-Phillips we shall now attempt to put the foregoing interpretation on a more rigorous basis. The convergence diagram in (K-P)[10] indicates that 22 plane waves gives nearly convergent term values for $X_1^{(2)}$ (conduction) and X_4 (valence), suggesting that the cancelation between the crystal potential Fourier components and the core-orthogonalization terms for these two levels is very satisfactory. As evidence of this a comparison can be made between the two sets of term values and the coefficients of the first few symmetrized OPW's in Table V which are obtained, first, by the perturbation method of Bassani-Celli[31] (which is the more sensitive of the two to a lack of cancellation) and, second, by solving a truncated secular equation. The energy eigenvalues obtained by these two methods agree within a few percent, although there are some differences between the amplitudes.

From the OPW's in Table V[32] (truncated secular equation) the squares of the amplitude of the eigenfunctions $X_{1g}^{(2)}$ and $X_{1u}^{(2)}$ (the smooth part only) are plotted in Fig. 7 along the [111] axis from the position of one atom at (000) towards that of the other atom at $(a/4, a/4, a/4)$. This plot of the electron probability density shows clearly that the wave function $X_{1g}(r)$ has no node along the axis, while $X_{1u}(r)$ has one node midway between the two neighboring atoms, i.e., at the point $\tau/2=(a/8, a/8, a/8)$. This property in addition to the "even" and "odd" character establishes the considerations of the previous section that the two eigenfunctions X_{1g} and X_{1u} have the symmetry character, *bonding* and *antibonding*, respectively, with respect to the interchange of the two atoms. A clearer understanding of the response of the X_1 electron to an applied

TABLE V. Calculated eigenvalues and coefficients (unnormalized) of OPW's for $X_1^{(2)}$ and X_4 obtained from the crystal potential Fourier components (k-independent exchange) and the orthogonalization coefficients of Kleinman-Phillips (see Refs. 10 and 32) from solution of a truncated secular equation using 22 plane waves. Numbers in brackets are the corresponding solution using Bassani-Celli's method.

Symmetrized OPW	⟨100⟩	⟨011⟩	⟨120⟩	⟨211⟩$_+$	⟨211⟩$_-$	Eigenvalues (Ry)
$X_1^{(2)}$	−0.251 (−0.432)	1.000 (1.000)	−0.152 (−0.083)	−0.185 (−0.138)	−0.092 (0)	−1.416 (−1.38)
X_4		1.000 (1.000)	0.358 (0.340)	−0.079 (0)		−1.731 (−1.77)

[30] J. C. Slater and G. F. Koster, Phys. Rev. **94**, 1498 (1954).

[31] F. Bassani and V. Celli, Phys. Chem. Solids **20**, 64 (1961).

[32] These were provided by L. Kleinman (private communication).

force of the type yz may be grasped by considering the connection between the energy eigenvalues and the number of nodes of the wave function. In the present situation the experimental result is consistent with the idea that when a crystal is compressed, the kinetic energy gain is larger for the plane wave having the greater number of nodes along the direction of compression.

In Table V both eigenfunctions $X_1^{(2)}$ and X_4 have their largest coefficient on the symmetrized $\langle 011\rangle$ OPW admixed to which are a few other waves with rather small amplitudes. This means that except in the core region the solutions for $X_1^{(2)}$ and X_4 are very nearly free-electron like[33] consistent with Phillips' pseudopotential results.[34] The energy gap between these two levels, which vanishes in the free-electron limit, therefore, is very sensitive to the small mixing effects.

If the *largest* plane wave $\langle 011\rangle$ alone were taken into account, the amplitude $|X_{1g}^{(2)}|^2$ in Fig. 7 would be constant along the [111] axis, while the amplitude $|X_{1u}^{(2)}|^2$ would be of sinusoidal character with a single nodal plane midway between the two atoms [see Eqs. (50) and (51)]. The mixing of the *adjacent* plane wave $\langle 100\rangle$ with the $\langle 011\rangle$ plane wave modifies this in an interesting way: The matrix element of the potential between the $\langle 011\rangle$ and $\langle 100\rangle$ waves is $\sqrt{2}V_{111}$, the Fourier component which Phillips has shown to be incompletely cancelled by the orthogonalization and responsible for the bonding action.[35] In fact, the effect of this potential component on the $\langle 011\rangle$ and $\langle 100\rangle$ waves makes their unperturbed energy separation larger (by raising the $\langle 011\rangle$ level and depressing the $\langle 100\rangle$ level) and, at the same time, imparts to the resulting two levels bonding and antibonding characters. This is clearly seen in Fig. 7 where $|X_{1g}^{(2)}(r)|^2$ decreases in the region between the two atoms rather than increases, indicating that the upper level $X_1^{(2)}$ has over-all antibonding character in regards to the s-p hybridization mentioned in Sec. VA [$\sin\vartheta\cos\vartheta<0$ in Eqs. (45a) and (45b)]. This leads to the conclusion that the energy interval $E(X_1^{(2)})-E(X_4)$ is determined largely by the uncancelled V_{111}.

Finally, it is interesting to compare the deformation potential $\Xi_{u'}$ (and the other two constants Ξ_d, Ξ_u) calculated directly from the knowledge of the wave function with the experimental results in Eq. (40). Such calculations have been undertaken by Goroff and Kleinman.[12] From the definitions in Eqs. (9) and (10) and the form $\delta H_{\text{strain}}(\text{1-electron})=D_{\mu\nu}S_{\mu\nu}$ the two shear-constants can be written

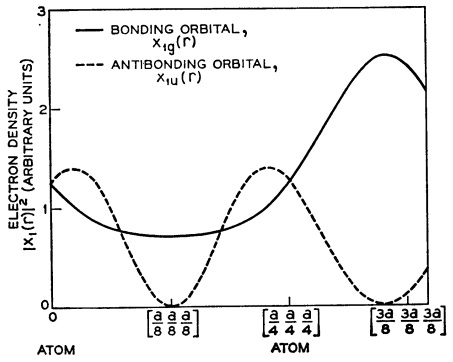

FIG. 7. The square of the conduction electron wave functions $|X_{1g}(r)|^2$ (bonding) and $|X_{1u}(r)|^2$ (antibonding) along the [111] axis in Si according to the OPW theory of Kleinman and Phillips. Twenty-two plane waves have been used to solve an OPW secular equation of 5×5 dimension. The results plotted omit the core oscillatory part.

$$\Xi_u(X_1)=\langle X_1|D_{xx}-D_{yy}|X_1\rangle, \tag{48}$$

$$\Xi_{u'}(X_1)=\langle X_1|D_{xy}|\bar{X}_1\rangle. \tag{49}$$

The one-electron operator $D_{\mu\nu}$ is a sum of the kinetic energy part and the potential part.[36] The kinetic part is of the form $-(1/m)p_\mu p_\nu$ which arises as a consequence of the *scaling* process[15,17] $p\rightarrow(1-s)p$. The question which has hitherto been asked[37] whether the kinetic part alone might give a predominant contribution to the actual deformation potential is tested by taking the first plane wave $\langle 011\rangle$, its symmetrized form being explicitly

$$X_1\langle 011\rangle=\frac{1}{i}\left(\cos\frac{2\pi}{a}(y+z)+i\cos\frac{2\pi}{a}(y-z)\right). \tag{50}$$

and

$$\bar{X}_1\langle 011\rangle=\frac{-1}{i}\left(\cos\frac{2\pi}{a}(y+z)-i\cos\frac{2\pi}{a}(y-z)\right). \tag{51}$$

[These satisfy IR's in Table I and the phase required in Eqs. (6) and (7).] From the first plane wave $\langle 011\rangle$ alone we obtain

$$\Xi_u(X_1)_{\text{kinetic}}=\Xi_{u'}(X_1)_{\text{kinetic}}\approx 0.7\ \text{Ry}(9.5\ \text{eV}). \tag{52}$$

These are compared with Goroff-Kleinman's more precise values[12] $\Xi_u(X_1)=9.57$ eV, $\Xi_{u'}(X_1)=7.8$ eV, in which *all* other corrections are included. The closeness between the kinetic part and the total for both Ξ_u and $\Xi_{u'}$ (especially for Ξ_u) is striking and suggests the insignificance of the potential correction in the case of the

[33] An additional argument supporting the approximate validity of the "free-electron" limit for $X_1^{(2)}$ and X_4 (at least as far as the eigenfunctions are concerned) is the fact that this picture is roughly consistent with the observed effective-mass values, Eqs. (30) and (31), for the conduction band edge. The use of the first plane wave $\langle 011\rangle$ alone gives $\langle X_1^{(2)}|p_x|X_1^{(2)}\rangle\approx 0$ and $\langle X_1^{(2)}|p_y|X_4\rangle\approx(2\pi/a)$, which according to Eqs. (15) and (16) yield the effective mass values $(m_{\parallel}/m_0)\approx 1$ and $(m_{\perp}/m_0)\approx 0.20$. The latter value, it should be mentioned, depends rather critically on the value of the energy gap (Ref. 22), $E(X_1^{(2)})-E(X_4)\approx 4.3$ eV.

[34] J. C. Phillips, Phys. Rev. **112**, 685 (1958).

[35] J. C. Phillips, *Proceedings of the International Conference on Semiconductor Physics, Prague, 1960* (Czechoslovak Academy of Sciences, Prague, 1961), p. 41.

[36] For details, see L. Kleinman, Phys. Rev. **128**, 2614 (1962).

[37] For a review on this subject see R. W. Keys, in *Solid State Physics*, edited by F. Seitz and D. Turnbull (Academic Press Inc., New York, 1960), Vol. **11**, p. 149.

conduction electron in Si.[38] This result might reflect, again, a nearly free-electron picture of (K-P) theory.

A comparison between the theoretical value and experimental ones for Ξ_u is made in Ref. 12. For $\Xi_{u'}$, the present estimate $\Xi_{u'}(k_0)=5.7\pm1$ eV from the experimental work is somewhat small compared to the theoretically deduced value, even if the difference between X and k_0 is taken into consideration.

ACKNOWLEDGMENTS

We would like to thank Professor Y. Uemura, Professor T. Inui, and Professor J. C. Phillips for helpful discussions. We are indebted to Dr. L. Kleinman for providing us results from his unpublished work. This work originated in a conversation which one of us (H. H.) had with Dr. L. M. Roth in 1960, to whom he would like to express his gratitude. He also would like to thank Dr. B. Lax and Dr. H. J. Zeiger for making his visit to Lincoln Laboratory possible. The assistance of D. H. Sweet in making the measurements is gratefully acknowledged.

APPENDIX A

The calculations of the two quantities $Z(k_x)$ and $Z'(k_x)$ defined by Eqs. (22) and (23) have been performed on the basis of the OPW theory discussed in Sec. VB. In the sense of lowest order perturbation theory the matrix element $\langle X_1^{(2)}|p_y|X_4\rangle$ may be calculated from

$$\langle X_1^{(2)}|p_y|X_4\rangle = (2\pi/a)[1-\tfrac{1}{2}\textstyle\sum_{\text{core}}(\langle\varphi_k X_c\rangle_{X_1}{}^2+\langle\varphi_k X_c\rangle_{X_4}{}^2)], \quad \text{(A1)}$$

where φ_k and X_c represent the symmetrized $\langle 011\rangle$ wave (not orthogonalized) and a corresponding core function. Equation (A1) is a consequence of normalization and an interference between the plane waves and the cores. Using the orthogonalization coefficients of (K-P),[32] we deduce the right-hand side of Eq. (A1) to be $(2\pi/a)\times0.94$. A more elaborate calculation including the terms of the next (second) order based on the results in Table V (Bassani-Celli) leads to a value only 10% smaller. In such a calculation the terms corresponding to core-core matrix elements are ignored. The contribution from these terms are at present not known. Inasmuch as the ratio f [Eq. (28)] is quite insensitive to the magnitude of $Z(X)=-Z'(X)$ (it only depends strongly on the relative magnitudes of these functions when corrected at k_0), we adopt the estimate $\langle X_1^{(2)}|p_y|X_4\rangle\approx(2\pi/a)\times0.9$ for the present discussion. This gives

$$Z(X)=-Z'(X)=0.96 \quad \text{(A2)}$$

using $E(X_1^{(2)})-E(X_4)=4.3$ eV.[22] In view of the difficulty in accurately determining $Z(k_0)$ and $Z'(k_0)$ it is advantageous for the purpose of analyzing the present experiments to find instead the best theoretical estimate of the ratio $f=Z'(k_0)/Z(k_0)$ whereby uncertainties common to Z and Z' tend to cancel. In calculating f the correction (first order in k_0) to the matrix elements $\langle\Delta_1|p_y|\Delta_5\rangle$ and $\langle\Delta_5|p_z|\Delta_{2'}\rangle$ due to the difference between k_0 and X is most significant. (Other corrections such as those arising from X_3 levels are found to be less than 2%.)

We have calculated this correction by considering

$$\langle\Delta_1|p_y|\Delta_5\rangle=\langle X_1^{(2)}|p_y|X_4\rangle+\delta_p, \quad \text{(A3)}$$

$$\langle\Delta_5|p_z|\Delta_{2'}\rangle=-\langle X_1^{(2)}|p_y|X_4\rangle+\delta_p, \quad \text{(A4)}$$

where

$$\delta_p=\frac{k_0}{m}\Big\{\sum_\nu \frac{1}{E(X_1^{(2)})-E(X_1^{(\nu)})}\langle X_1^{(2)}|p_x|X_1^{(\nu)}\rangle \times\langle X_1^{(\nu)}|p_y|X_4\rangle+\sum\frac{1}{E(X_4)-E(X_3^{(\nu)})} \times\langle X_1^{(2)}|p_y|X_3^{(\nu)}\rangle\langle X_3^{(\nu)}|p_y|X_4\rangle\Big\}. \quad \text{(A5)}$$

By inspection the dominant contribution to this expression is

$$\frac{k_0/m}{E(X_1^{(2)})-E(X_1^{(1)})}\langle X_1^{(2)}|p_x|X_1^{(1)}\rangle\langle X_1^{(1)}|p_y|X_4\rangle,$$

which has been evaluated using the OPW's discussed earlier in Sec. VB, yielding

$$\delta_p\approx0.03(2\pi/a). \quad \text{(A6)}$$

The theoretical uncertainty of this number stems mainly from the inaccuracy of the term difference $E(X_1^{(2)})-E(X_1^{(1)})$, to which the uncertainty of the exchange dependence contributes most significantly.[10] However, since we see that $\delta_p\ll\langle X_1^{(2)}|p_y|X_4\rangle$, the uncertainty of δ_p causes no serious error in the sums in Eqs. (A3) and (A4) used to obtain $\langle\Delta_1|p_y|\Delta_5\rangle$ and $\langle\Delta_5|p_z|\Delta_{2'}\rangle$. Taking into account this theoretical uncertainty reasonably we get

$$\langle\Delta_5|p_z|\Delta_{2'}\rangle/\langle\Delta_1|p_y|\Delta_5\rangle=-0.94\pm0.02, \quad \text{(A7)}$$

which we have quoted in Eq. (29).

[38] L. Kleinman has stated that for the valence band hole this is not the case. See Ref. 36.